Product Branching from the CH2CH2OH Radical Intermediate of the OH plus Ethene Reaction

ARTICLE *in* THE JOURNAL OF PHYSICAL CHEMISTRY A · AUGUST 2011

Impact Factor: 2.69 · DOI: 10.1021/jp203127k · Source: PubMed

5 AUTHORS, INCLUDING:

Jim J Lin
Academia Sinica
121 PUBLICATIONS **2,715** CITATIONS

SEE PROFILE

THE JOURNAL OF PHYSICAL CHEMISTRY A

ARTICLE

pubs.acs.org/JPCA

Product Branching from the CH_2CH_2OH Radical Intermediate of the OH + Ethene Reaction

Britni J. Ratliff, Bridget W. Alligood, and Laurie J. Butler*

The James Franck Institute and Department of Chemistry, University of Chicago, Chicago, Illinois 60637, United States

Shih-Huang Lee

National Synchrotron Radiation Research Center, Hsinchu, 30076 Taiwan, Republic of China

Jim Jr-Min Lin

Institute of Atomic and Molecular Sciences, Academia Sinica, Taipei, 10617 Taiwan, Republic of China

Supporting Information

ABSTRACT: Using a crossed laser-molecular beam scattering apparatus and tunable photoionization detection, these experiments determine the branching to the product channels accessible from the 2-hydroxyethyl radical, the first radical intermediate in the addition reaction of OH with ethene. Photodissociation of 2-bromoethanol at 193 nm forms 2-hydroxyethyl radicals with a range of vibrational energies, which was characterized in our first study of this system (*J. Phys. Chem. A* **2010**, *114*, 4934). In this second study, we measure the relative signal intensities of ethene (at $m/e = 28$), vinyl (at $m/e = 27$), ethenol (at $m/e = 44$), formaldehyde (at $m/e = 30$), and acetaldehyde (at $m/e = 44$) products and correct for the photoionization cross sections and kinematic factors to determine a 0.765:0.145:0.026:0.063:<0.01 branching to the OH + C_2H_4, H_2O + C_2H_3, CH_2CHOH + H, H_2CO + CH_3, and CH_3CHO + H product asymptotes. The detection of the H_2O + vinyl product channel is surprising when starting from the CH_2CH_2OH radical adduct; prior studies had assumed that the H_2O + vinyl products were solely from the direct abstraction channel in the bimolecular collision of OH and ethene. We suggest that these products may result from a frustrated dissociation of the CH_2CH_2OH radical to OH + ethene in which the C−O bond begins to stretch, but the leaving OH moiety abstracts an H atom to form H_2O + vinyl. We compare our experimental branching ratio to that predicted from statistical microcanonical rate constants averaged over the vibrational energy distribution of our CH_2CH_2OH radicals. The comparison suggests that a statistical prediction using 1-D Eckart tunneling underestimates the rate constants for the branching to the product channels of OH + ethene, and that the mechanism for the branching to the H_2O + vinyl channel is not adequately treated in such theories.

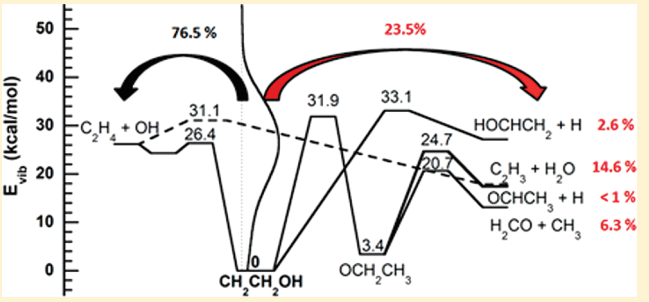

INTRODUCTION

Due to the importance of the reaction of OH radicals with alkenes in combustion and atmospheric chemistry, the reaction of OH with ethene has been the focus of over fifteen theoretical and forty-five experimental studies.[1−17] The early temperature- and pressure-dependent rate studies[8−10] found that, at high temperatures, the reaction results in direct H-atom abstraction to form H_2O + vinyl while, at low temperatures, the reaction is dominated by the addition of the OH to the double bond of ethene. Tully[9,10] concluded that the radical adduct formed by the addition mechanism primarily redecomposes to OH + ethene rather than branching to the energetically allowed product channels. Master equation modeling[11,12] provided comparisons with subsequent studies of the product branching, but one study[11] had a high barrier to the direct abstraction channel and so concluded it was unimportant, and the other[12] did not include an ethenol + H product channel in its analysis. When later flame studies[13,14] detected ethenol products, the interest in the OH + ethene reaction was renewed. The most recent theoretical study[2] of the competition between the isomerization and decomposition pathways of the CH_2CH_2OH radical adduct is by Senosiain et al. On their calculated potential energy surface shown in Figure 1, the CH_2CH_2OH radical intermediate has two possible direct dissociation channels; it may redissociate to OH + ethene or undergo direct C−H bond fission to form ethenol + H. Alternatively, the radical may isomerize to the ethoxy radical and undergo either C−C bond fission to form H_2CO + CH_3 or C−H bond fission to form CH_3CHO + H. To our knowledge, two

Received: April 4, 2011
Revised: June 15, 2011
Published: July 12, 2011

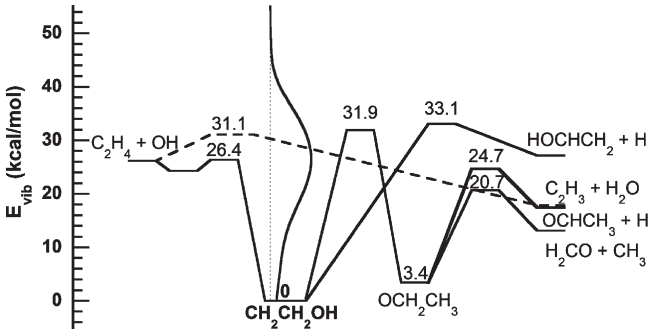

Figure 1. Vibrational energy for all nascent CH_2CH_2OH radicals formed in the photodissociation of 2-bromoethanol at 193 nm. This distribution is superimposed on the critical points on the potential energy surface calculated by Senosiain et al.[2] and is reproduced from Figure 10 of ref 1, copyright 2010 American Chemical Society.

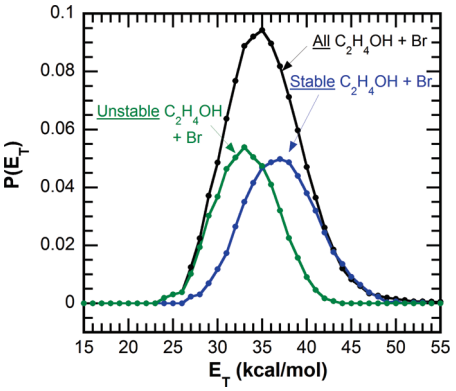

Figure 2. Recoil kinetic energy distribution, $P(E_T)$, for C−Br bond fission events that result in Br + all CH_2CH_2OH radicals (solid black line), Br + stable CH_2CH_2OH radicals (solid blue line), and Br + unstable CH_2CH_2OH radicals (solid green line) as measured in our previous velocity map imaging experiments on the photodissociation of 2-bromoethanol at 193 nm. The $P(E_T)$ for Br + unstable CH_2CH_2OH radicals is obtained by subtracting the $P(E_T)$ for Br + stable CH_2CH_2OH radicals (measured from the detection of CH_2CH_2OH photofragments at $m/e = 45$) from the $P(E_T)$ for all Br + CH_2CH_2OH radicals (measured from the detection of Br photofragments at $m/e = 79$). Adapted from Figure 6a of ref 1, copyright 2010 American Chemical Society.

studies[15,16] have experimentally measured the product branching from the OH + ethene reaction. The first study[15] reported the temperature dependence of the high−pressure limiting rate coefficients and the pressure dependent yield of $H_2CO + CH_3$ at high pressures, while the other[16] determined that collisions between OH and ethene at 2 Torr of He and 295 K result in 44% formaldehyde, 21% stabilized CH_2CH_2OH adduct, and 35% C_2H_4O, which was attributed completely to an acetaldehyde + H product channel (at that time, dissociation to ethenol + H was not considered).

As the branching to the product asymptotes accessible to the CH_2CH_2OH radical adduct is critically dependent on the vibrational energy distribution of the radical, in our first study of this system[1] we characterized the vibrational energy distribution of the CH_2CH_2OH radical intermediate when it is formed from the 193 nm photodissociation of 2-bromoethanol. We first measured the recoil kinetic energy distribution, $P(E_T)$, for all C−Br bond fission events by state-selectively detecting, with 2 + 1 resonance enhanced multiphoton ionization (REMPI), the momentum matched $Br(^2P_{3/2})$ and $Br(^2P_{1/2})$ cofragments to the radicals of interest. We then detected the stable CH_2CH_2OH radicals with 118 nm photoionization to determine the $P(E_T)$ for photodissociation events resulting in Br + stable CH_2CH_2OH. As shown in Figure 2, the difference between the $P(E_T)$ for Br + all CH_2CH_2OH radicals and the $P(E_T)$ for Br + stable CH_2CH_2OH radicals gives a $P(E_T)$ for photodissociation events producing Br + unstable CH_2CH_2OH radicals, which can undergo subsequent dissociation. A rotating source, scattering experiment with electron bombardment detection by Lee and co-workers[3] also measured the translational energy distributions for Br + all CH_2CH_2OH radicals and Br + stable CH_2CH_2OH radicals, which agree with our $P(E_T)$'s on the fast edge but show more photodissociation events with lower recoil kinetic energy. Because our imaging experiments were able to state-selectively detect the Br spin−orbit states, which differ in energy by 10.5 kcal/mol, we use these $P(E_T)$'s and their corresponding measured anisotropy to characterize the primary photodissociation process while fitting the data reported herein.

Using momentum and energy conservation, we determined the internal energy distribution of all nascent CH_2CH_2OH radicals from the measured $P(E_T)$ for Br + all CH_2CH_2OH radicals. To characterize the vibrational energy distribution of the nascent radicals, we introduced an impulsive model that accounts for zero-point and thermal vibrational motion of the photolytic precursor. The model predicts the energy partitioned to rotation of the CH_2CH_2OH radical by using our measured translational energy distribution, while assuming an impulsive C−Br fission and averaging over the distribution of exit impact parameters due to the normal mode corresponding to the C−C−Br bend. We account for two isomers of 2-bromoethanol; the best fit arises by assuming 80% of the molecules dissociate from a conformer that is trans about the C−C bond and 20% from a conformer that is gauche about the C−C bond. The model was validated by comparing the predicted recoil kinetic energy of Br + stable CH_2CH_2OH radicals (those formed with vibrational energy below the lowest dissociation barrier) with that measured in our imaging experiment. After resolving the portion of internal energy that was partitioned to rotation, we determined the vibrational energy distribution for all nascent CH_2CH_2OH radicals, as shown in Figure 1, which is reproduced from our previous publication[1] and shown superimposed on the potential energy surface calculated by Senosiain et al.[2]

Here we present the first complete product study of the branching between the dissociation channels accessible to 2-hydroxyethyl radical when formed with the vibrational energy distribution shown in Figure 1. As expected, we detect ethenol + H, $H_2CO + CH_3$, and OH + ethene product signal. Both ethenol and acetaldehyde products may give signal at the mass to charge ratio (m/e) of 44. In a flame study, Cool et al.[18] determined the isomeric composition by measuring the photoionization efficiency (PIE) curve. At each ionization energy, the total observed signal is a linear combination of the mole fraction of each isomer, weighted by its partial photoionization cross section. We used this technique to determine the branching between the ethenol + H and acetaldehyde + H product channels. Our data surprisingly showed significant signal from one channel, H_2O + vinyl, that is not expected to be accessible from the

CH_2CH_2OH radical adduct. Independent and concurrent work by Bowman and co-workers[4] found trajectories to H_2O + vinyl that start from the CH_2CH_2OH radical during what appears to be a frustrated dissociation to OH + ethene. Because the dissociation to OH + ethene is over a flat region of the potential energy surface typically treated by variational transition state theory, we infer that the OH group can recross to abstract an H atom and form H_2O + vinyl products.

EXPERIMENTAL METHOD

The velocity distributions of the photofragments of 2-bromoethanol and the products of the unimolecular decomposition of the CH_2CH_2OH radical intermediate were measured using the rotating source, crossed laser-molecular beam apparatus[19−23] at the 21A1 U9/Chemical Dynamics Beamline at the National Synchrotron Radiation Research Center (NSRRC) located in Hsinchu, Taiwan. The molecular beam was formed by seeding the equilibrium vapor pressure of 2-bromoethanol (97% purity, Alfa Aesar) at 40 °C in He gas to a total stagnation pressure of 860 Torr. The beam expanded through an Even-Lavie pulsed valve with a 0.25 mm orifice diameter and cone-shaped exit port. The valve was heated to 75 °C and pulsed with a 30 μs open time at a rate of 80 Hz. The molecular beam intersected the unpolarized output of a Lambda Physik LPX 220 ArF laser, operating at 193.3 nm, which photodissociated 2-bromoethanol to produce momentum-matched Br atoms and 2-hydroxyethyl radical photofragments. The measured pulse energy for each spectrum ranged from 12 to 15 mJ per pulse, well below the saturation level of 2-bromoethanol (its absorption cross section is $\sim 10^{-19}$ cm^2 per molecule). The beam spot was rectangular in shape, 3 mm tall and 2 mm wide. A small number of the recoiling photofragments traveled a neutral flight distance of 10.05 cm to the ionization region, where they were ionized with tunable vacuum ultraviolet (VUV) synchrotron radiation. Ionization energies were chosen by tuning the U9 undulator gap, and the VUV beam was defined by a 7 mm diameter circular aperture. (Refer to our previous publication[24] for a discussion of the recalibration of the undulator gap and interpretation of bandwidth-averaged cross sections.) Higher harmonics of the VUV radiation were filtered out using a rare gas filter (Xe, Kr, Ar, or He depending on the range of photoionization energy) at a pressure of 10 Torr. After traveling to the ionizing region, the photofragments were ionized and mass selected using an Extrel 1.2 MHz (2.9 MHz for H atom detection) quadrupole mass spectrometer and were counted with a Daly detector.[25] A multichannel scaler recorded the total time-of-flight (TOF) of the photofragments traveling from the interaction region to the Daly detector. The flight times depicted in the figures are the sum of the neutral photofragment flight time (determined by the vector sum of the center-of-mass velocity, the recoil velocity imparted to the photofragment in the photodissociation, and any additional velocity imparted to the products from the dissociation of the nascent unstable radicals) and the ion flight time through the mass spectrometer. The latter is calculated using the apparatus' measured ion flight constant of 5.36 μs $amu^{-1/2}$. All of the TOF spectra were accumulated in 0.5 μs channels, and their associated fits are corrected for the 2.10 μs timing offset between the triggering of the multichannel scalar and the later arrival of the laser pulse at the crossing point of the laser and the molecular beam. Time-of-flight spectra were accumulated for HBr^+ (m/e = 82), Br^+ (m/e = 79), $CH_2CH_2OH^+$ (m/e = 45), $C_2H_2OH^+$ (m/e = 43), CH_2OH^+ (m/e = 31), H_2CO^+ (m/e = 30), HCO^+ (m/e = 29), $C_2H_4^+$ (m/e = 28), $C_2H_3^+$ (m/e = 27), $C_2H_2^+$ (m/e = 26), OH^+ (m/e = 17), CH_3^+ (m/e = 15), and H^+ (m/e = 1). A year later, we returned to the NSRRC to accumulate signal at H_2O^+ (m/e = 18). At that time, a LPF 200, Lambda Physik Laser Tecknik laser with beam spot of 4 mm × 3 mm and pulse energy of approximately 120 mJ/pulse was used for the 193 nm photodissociation of 2-bromoethanol, and the timing offset between the triggering of the multichannel scalar and the later arrival of the laser pulse at the crossing point of the laser and molecular beam was measured to be 1.1 μs. The other experimental conditions remained the same.

The speed distribution of the molecular beam was measured using a chopper wheel rotating at 200 Hz that was placed nominally 6.75 cm from the detector. The velocity distribution, $N(v)$, displayed a slow tail that was not fit by the standard expression $N(v) = v^2 \exp[-(v/\alpha - S)^2]$, where α and S are fitting parameters. We took great care to characterize the entire velocity distribution of the molecular beam by treating the beam as though it were composed of a fast and slow velocity distribution, the sum of which yields the entire observed velocity distribution; more details regarding this analysis are in the Supporting Information. The peak in the number density distribution of molecular speeds was 16.5 × 10^4 cm/s with a full width at half-maximum of 19%.

We also measured the photoionization efficiency (PIE) curve from 7.3 to 14.6 eV of the m/e = 44 signal resulting from the 193 nm photodissociation of 2-bromoethanol. Due to the need to change the filter gas over the broad range of photoionization energies, this PIE curve was measured in three overlapping segments (three passes from 7.3 to 9.2 eV with Xe as the filter gas, six passes from 8.8 to 12.2 eV with Kr as the filter gas, and three passes from 11.7 to 14.6 eV with Ar as the filter gas) that were scaled, respectively, to give the total PIE curve using the overlapping data points as described in the Supporting Information. During each pass, the m/e = 44 signal was accumulated for 50 000 laser shots at each ionization energy. Because the NSRRC bandwidth, with an aperture size of 7 mm, is considerably broader than that used in the high resolution experiments by Cool and co-workers,[18] we also measure the PIE curve for pure acetaldehyde, shown in the Supporting Information, from 8.4 to 12.7 eV with Kr as the filter gas. Due to its high vapor pressure, the acetaldehyde was cooled to −24 °C and seeded in He to a total stagnation pressure of 900 Torr.

Fitting the data presented herein was complicated by difficulties pertaining to the precise characterization of the ion flight time and the initial molecular beam velocity. Evidence of these difficulties can be seen throughout the figures: the fits for m/e = 79 (Br^+) as a function of angle do not match the data on the fast edge, and the signal from dissociative ionization is slightly faster and sometimes broader than the predicted fits. (The Supporting Information shows data from SF_6, which shows that dissociative ionization from higher harmonics may create ions with a broader time-of-flight distribution than the parent ion from the same neutral species.) Fortunately, the integrated relative signal intensities between products proved insensitive to small changes in these parameters, and we are thus able to comfortably report the branching between the product channels observed from the CH_2CH_2OH radical adduct. The error bars for the partial photoionization cross section of each species far exceeds the uncertainty in relative signal intensities.

Table 1. Appearance Energies of Detected Mass-to-Charge Ratios (m/e) from the Neutral Species[a]

detected m/e	ionization photon energy (eV)	potential signal contributors ion/neutral (appearance energy)
79	15.34	Br^+/Br (11.81)
82	15.34	HBr^+/HBr (11.7)
45	10.5	$CH_2CH_2OH^+/CH_2CH_2OH$ (6.5)
	11.27	$CH_2CH_2OH^+/CH_2CH_2OH$ (6.5)
44	9.2	CH_2CHOH^+/CH_2CHOH (9.3)
	11.27	CH_3CHO^+/CH_3CHO (10.2), CH_2CHOH^+/CH_2CHOH (9.3), CH_3CHO^+/CH_2CH_2OH (11.0), CH_2CHOH^+/CH_2CH_2OH (10.5)
30	11.27	H_2CO^+/H_2CO (10.88), *H_2CO^+/CH_2CH_2OH (11.5), H_2CO^+/CH_2CHOH (15.3)*
28	11.27	$C_2H_4^+/C_2H_4$ (10.51), *$C_2H_4^+/CH_2CH_2OH$ (11.7)*
27	11.27	$C_2H_3^+/C_2H_3$ (8.25), $C_2H_3^+/CH_2CH_2OH$ (9.5), *$C_2H_3^+/CH_2CHOH$ (13.3)*
18	13.58	H_2O^+/H_2O (12.62)
17	13.58	OH^+/OH (13[a]), *OH^+/CH_2CHOH (19.9)*
15	11.27	CH_3^+/CH_3 (9.84[a]), CH_3^+/CH_2CH_2OH (10.4), *CH_3^+/CH_2CHOH (12.9)*

[a] Values shown in italics indicate that dissociative ionization that is not allowed at the ionization photon energy used for detection at the indicated mass-to-charge ratio but, nevertheless, was observed due to ionization with higher harmonics.

COMPUTATIONAL METHOD

To aid in the data analysis, the appearance energies of the detected m/e from the neutral species are shown in Table 1. When previous experimental or theoretical values were not known, we calculated the appearance energy at the G4//B3LYP/6-311++G(3df,2p) level of theory. Optimized molecular geometries and vibrational frequencies were found using the B3LYP density functional and the 6-311++G(3df,2p) basis set. The geometries converged to a root-mean-square (rms) force below 1×10^{-5} and an rms displacement below 4×10^{-5}, where both are in atomic units. Wave functions for doublet species were spin-unrestricted, and wave functions for singlet species were spin-restricted. The computation of the zero-point vibrational energies used the B3LYP/6-311++G(3df,2p) vibrational frequencies scaled by 0.9854, as Curtiss et al. recommended[26] and the G4 method required.[27] The G4 method is the latest in the series of Gn theories, which are composite methods based on a sequence of single point energy calculations. The calculations use the Gaussian 09 program, version A.02.[28]

RESULTS

A. Primary Photodissociation Channels.

1. C−Br Bond Fission of 2-Bromoethanol. Figure 3 shows the time-of-flight (TOF) spectra taken at m/e = 79 (Br^+) at three source angles: 20°, 30°, and 40°. The black solid line shows the predicted time-of-flight for Br atoms at each source angle if the C−Br bond fission of 2-bromoethanol is characterized by the recoil kinetic energy distribution, $P(E_T)$, measured in our previous imaging experiment (shown as the black line in Figure 2). The comparison of the predicted fits with the measured data as a function of angle suggests that the molecular beam velocity is only marginally inaccurate. We unsuccessfully attempted to iteratively adjust the molecular beam velocity to compensate for this angle dependence but could not obtain better agreement with the data. Given the error bars of the calibrated ion flight constant and beam velocity, this difference is within the uncertainty in these parameters. At the 20° source angle, the predicted time-of-flight agrees well with the data on the fast side but underpredicts the slower signal. The $P(E_T)$ for C−Br bond fission resulting from the 193 nm photodissociation of 2-bromoethanol measured in Lee and co-workers'[3] rotating source, scattering experiment with electron bombardment detection also observed additional slow signal, similar to what we see in the NSRRC data. Thus their forward convoluted $P(E_T)$ predicts additional photofragments with slower recoil kinetic energies. If we take a weighted sum of the imaging $P(E_T)$ and the additional signal detected by Lee and co-workers, we can get a better set of fits to the m/e = 79 signal, as shown in the Supporting Information. However, the difference between the two $P(E_T)$'s proves to be negligible in the subsequent analysis of product branching, as the secondary fits are relatively insensitive to small changes in the primary $P(E_T)$; see Supporting Information. Thus, we choose to use the imaging $P(E_T)$ for all C−Br bond fission events, because the imaging experiment resolved the $Br(^2P_{1/2})$ and $Br(^2P_{3/2})$ velocity distributions separately. We also considered the possibility that this additional signal may be from the photodissociation of molecular clusters in the beam, but the time of arrival of the signal is too fast, and the G4//B3LYP/6-311++G(3df,2p) appearance energy for m/e = 79 from 2-bromoethanol is 16.15 eV, which is higher than the photoionization energy used.

The TOF spectrum for m/e = 45 ($CH_2CH_2OH^+$) at 10.5 eV is shown in Figure 4 and is well fit using the $P(E_T)$ for Br + stable CH_2CH_2OH radicals determined in ref 1 and shown as the blue line in Figure 2. We also detect the dissociative ionization of the stable mass 45 radicals to m/e = 43 and 31, as expected given the appearance energies of 11.3 and 12.0 eV, respectively. These spectra and corresponding fits are given in the Supporting Information. We also see dissociative ionization of stable mass 45 radicals to m/e = 30 (AE = 11.5 eV), 28 (AE = 11.7 eV), and 27 (AE = 9.5 eV) at a photoionization energy of 11.27 eV; these spectra are shown in the sections below.

2. HBr Loss from 2-Bromoethanol. Figure 5 shows the TOF spectrum for m/e = 82 (HBr^+). We used forward convolution fitting of that signal to determine the recoil translational energy distribution shown in Figure 6 for the HBr photoelimination from 2-bromoethanol. Preliminary results from our ongoing study of 2-bromoethanol-1,1,2,2-d_4,[29] which has all of the hydrogen atoms replaced with deuterium except for the hydroxyl hydrogen, indicate that there are two mechanisms for HBr elimination from 2-bromoethanol, one that involves the loss of the hydroxyl hydrogen and another from the loss of a hydrogen atom from

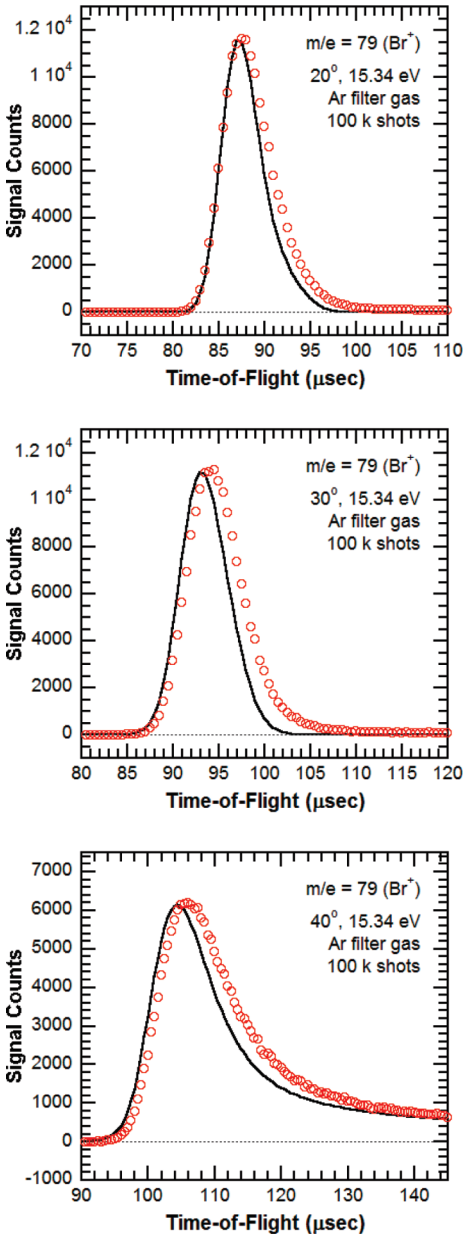

Figure 3. Time-of-flight spectra taken with a 20°, 30°, and 40° source angle, respectively, at m/e = 79 (Br^+) of the signal resulting from the C—Br bond fission of 2-bromoethanol at 193 nm. The forward convolution fit is predicted using the recoil kinetic energy distribution, $P(E_T)$, shown as a black solid line in Figure 2. The slight shift in the fit relative to the data as a function of angle represents an error in the molecular beam velocity but is well within the uncertainty of the experimental parameters.

the alkyl moiety. These two processes have very different recoil kinetic energies; the HBr elimination pathway that involves a hydroxyl hydrogen peaks at a much faster recoil kinetic energy. We have used this additional information to roughly divide our HBr elimination $P(E_T)$ into contributions from two channels. (The contributing $P(E_T)$'s shown in Figure 6 differ from those in ref 29 by a 4 kcal/mol shift to higher recoil kinetic energies. While the branching to HBr elimination was larger than DBr elimination in the 2-bromoethanol-1,1,2,2-d_4 study, the fit in Figure 5 required us to lower the relative contribution from HBr elimination of

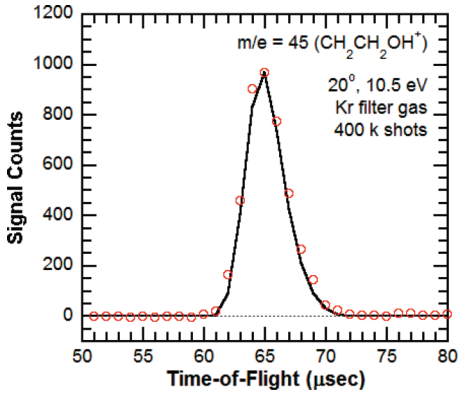

Figure 4. Time-of-flight spectrum at m/e = 45 ($CH_2CH_2OH^+$) of the stable CH_2CH_2OH radical products from the photodissociation of 2-bromoethanol. The open circles show the experimental data while the fit shown by the solid black line is a forward convolution fit using the $P(E_T)$ measured in our prior imaging experiments and shown as a solid blue line in Figure 2.

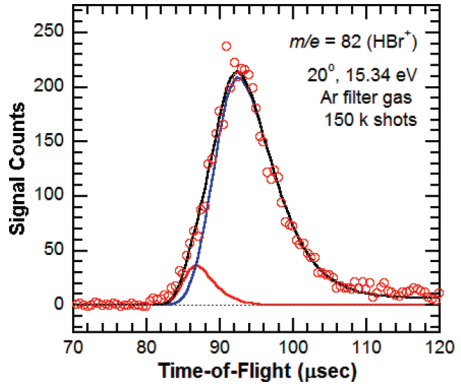

Figure 5. Time-of-flight spectrum taken at m/e = 82 (HBr^+) of HBr photofragments resulting from the minor HBr elimination channel. The forward convolution fit shown by the black solid line is the sum of the contribution from two HBr elimination channels, one in which the hydroxyl hydrogen is removed (red) and the other in which an alkyl hydrogen is removed (blue). These fits were obtained using the $P(E_T)$'s shown in Figure 6.

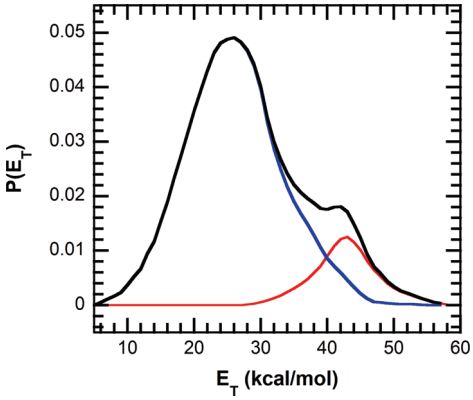

Figure 6. $P(E_T)$ for HBr loss from 2-bromoethanol from the forward convolution fits shown in solid line in Figure 5 for HBr photofragments detected at m/e = 82. The HBr elimination pathway that removes a hydroxyl hydrogen is shown as a red solid line, and the HBr elimination pathway that removes a hydrogen from the alkyl moiety is shown as a blue solid line.

dx.doi.org/10.1021/jp203127k |J. Phys. Chem. A 2011, 115, 9097–9110

2-bromoethanol from the hydroxyl hydrogen by a factor of 9.) In Figure 6, the $P(E_T)$ given by the red solid line, which peaks at 42 kcal/mol, is a five-center elimination that gives HBr products from the loss of the hydroxyl hydrogen. The $P(E_T)$ shown by the blue solid line peaks near 26 kcal/mol and can result from a three- or four-center HBr elimination.

3. Branching between the Photodissociation Channels. At a photoionization energy of 15.34 eV, we measured the branching ratio between C−Br bond fission and HBr loss from the 193 nm photodissociation of 2-bromoethanol. We accumulated signal at m/e = 79 and m/e = 82, alternating between the two in 25 000 laser shot increments to account for any drifts in laser intensity. Because some of the detected Br^+ signal could be from the dissociative ionization of HBr photofragments, we calculate the bandwidth-averaged partial photoionization cross sections at 15.34 eV to be $\sigma_{HBr^+/HBr}$ = 40.0 Mb and $\sigma_{Br^+/HBr}$ = 3.1 Mb from the data given in ref 30. Note that the $\sigma_{Br^+/HBr}$ cross section of 3.1 Mb assumes that the photoionization cross section for producing Br^+ ions from vibrationally excited HBr is the same as that for room temperature HBr. This is not likely to be true and thus we also assess the maximum contribution to Br^+ signal from dissociative ionization of HBr using the maximum photoionization cross section for $\sigma_{Br^+/HBr}$ of 10.74 Mb. Integrating the total fit in Figure 5 gives 4929 HBr^+ signal counts in 150 000 laser shots. Using the ratio of the partial photoionization cross sections in the equation below, we predict that 344 of the signal counts detected in 125 000 laser shots at m/e = 79 would be from the dissociative ionization of neutral HBr fragments to Br^+.

$$\left(\frac{4929 \text{ counts at } m/e = 82\ (HBr^+)}{150000 \text{ laser shots}}\right)\left(\frac{3.1 \text{ Mb } (\sigma_{Br^+/HBr})}{37.0 \text{ MB } (\sigma_{HBr^+/HBr})}\right) \times (125000 \text{ laser shots}) = 344 \text{ counts } Br^+/HBr$$

If we instead assume that vibrationally excited HBr has a partial photoionization cross section of $\sigma_{Br^+/HBr}$ = 10.74 Mb, then we expect 1192 signal counts of Br^+ from dissociative ionization of HBr. The inclusion of this minor contribution is not noticeable in the overall fit to the m/e = 79 data, as shown in the Supporting Information, but we do take it into consideration when determining the overall branching between C−Br bond fission and HBr elimination resulting from the photodissociation of 2-bromoethanol. Integrating the signal underneath the fit in the Supporting Information, which fits all of the m/e = 79 data, gives 198 774 signal counts in 125 000 laser shots at m/e = 79 (Br^+). We estimate the partial photoionization cross section for Br at 15.34 eV as 45.4 Mb.[31]

$$\frac{\Phi_{C-Br \text{ fission}}}{\Phi_{HBr \text{ loss}}} = \left(\frac{\text{integrated counts at } Br^+ - Br^+/HBr \text{ counts}}{\text{integrated counts at } HBr^+}\right) \times \left(\frac{\text{laser shots for } HBr^+ \text{ spectrum}}{\text{laser shots for } Br^+ \text{ spectrum}}\right) \times \left(\frac{\text{expected } HBr^+ \text{ signal}}{\text{expected } Br^+ \text{ from Br atom signal}}\right)\left(\frac{\sigma_{HBr^+/HBr}}{\sigma_{Br^+/Br}}\right) = \left(\frac{198774 - 344}{4929}\right)\left(\frac{150000}{125000}\right)\left(\frac{184049}{130687}\right)\left(\frac{36.96}{45.4}\right) = \frac{55.4}{1}$$

The resulting experimental branching ratio shows that 98.2% of the 2-bromoethanol molecules undergo C−Br bond fission while 1.8% undergo HBr loss. Our prior 200 eV electron bombardment ionization measurements[1] and the previous experiment by Lee and coworkers[3] were unable to detect the small branching to this channel.

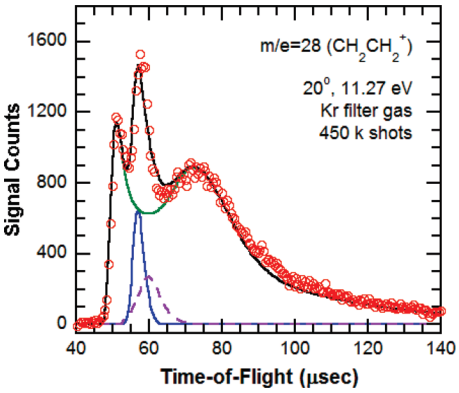

Figure 7. Time-of-flight spectrum at m/e = 28 ($C_2H_4^+$) detected with 11.27 eV ionization. The data are shown as open circles. The fit shown by the solid green line represents C_2H_4 products formed when CH_2CH_2OH radicals undergo subsequent dissociation to C_2H_4 + OH with the $P(E_T)$ shown in Figure 8. The solid blue line is the signal from the dissociative ionization of stable CH_2CH_2OH radicals. A possible contribution from dissociative ionization of HBr to m/e = 44 is shown by the dashed purple line, calculated from the $P(E_T)$ in Figure 6.

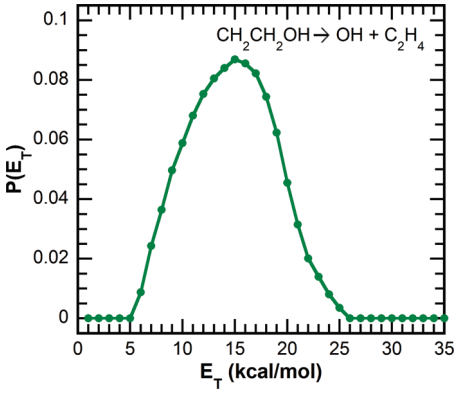

Figure 8. Recoil kinetic energy distribution, $P(E_T)$, for the dissociation of CH_2CH_2OH to C_2H_4 + OH derived from forward convolution fitting the m/e = 28 and m/e = 17 signal in Figures 7 and 10, respectively. The $P(E_T)$ peaks at 15 kcal/mol. An impulsive model, in which all of the rotational energy of the CH_2CH_2OH radicals is imparted to translational energy of the products during C−O bond fission, predicts E_T = 17.1 kcal/mol, which is in agreement with the $P(E_T)$ obtained from the forward-convolution fitting of the signal.

B. Detection of OH + Ethene Products at *m/e* = 17 and *m/e* = 28. As shown in Figure 1, the OH + ethene reactant asymptote is the one with the lowest energy barrier, 26.4 kcal/mol, accessible to vibrationally excited CH_2CH_2OH radicals. The TOF spectrum for ethene products detected at m/e = 28 is shown in Figure 7. The fit given by the solid green line results from forward convolution fitting, adding the velocity of the nascent unstable radicals determined from the green line $P(E_T)$ in Figure 2 to the velocity of the C_2H_4 products from the secondary dissociation of the radicals. The $P(E_T)$ shown in Figure 8 for $CH_2CH_2OH \rightarrow$ OH + ethene characterizes the secondary dissociation process. When forward convolution fitting the spectrum, we must also define the angular distribution

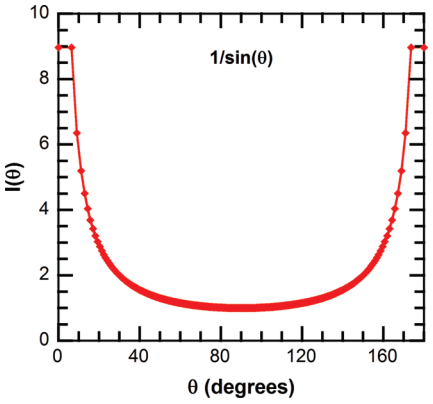

Figure 9. Angular distribution for the dissociation of CH_2CH_2OH radicals to three product channels: OH + ethene, H_2CO + CH_3, and vinyl + H_2O. The angle θ is the angle between the velocity vector, in the center of mass reference frame, of the radical that dissociates and the direction of recoil of the detected product from that dissociation. This angular distribution is based on the assumption that the dissociation lifetime of the radical is long with respect to its rotational period and that it is coplanar. The flattening of the function near 0° and 180° approximately accounts for small noncoplanar forces in the dissociation of the rotating radicals.

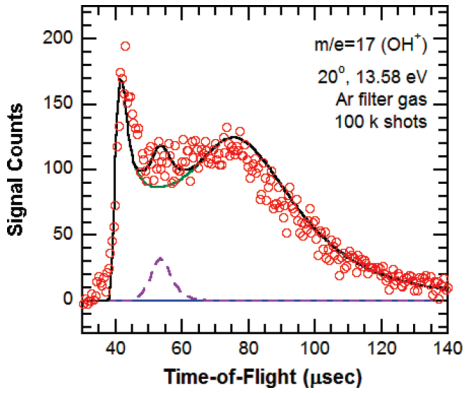

Figure 10. Time-of-flight spectrum at m/e = 17 (OH^+) detected with 13.58 eV. The data are shown as open circles, and the solid green line shows the OH^+ signal from OH products from the dissociation of CH_2CH_2OH to C_2H_4 + OH and is momentum matched to the signal shown by the solid green line in Figure 7. A small signal near 55 μs suggests a possible contribution from the dissociative ionization of m/e = 44 photofragments from HBr elimination from 2-bromoethanol, shown by the dashed purple line.

$I(\theta)$, where $I(\theta)$ sin θ dθ dφ gives the differential scattering of the secondary product's velocity vector with respect to the velocity of the dissociating CH_2CH_2OH radical. Assuming that the dissociation lifetime of the radical is long with respect to its rotational period, we set $I(\theta) = 1/\sin(\theta)$, truncated near 0° and 180° as shown in Figure 9. This gives an angular distribution that is symmetric and strongly forward−backward peaked, as would be expected for the dissociation of highly rotationally excited CH_2CH_2OH radicals. (A rough RRKM calculation for the rate of dissociation to OH + ethene using the 26.4 kcal/mol transition state predicts that the dissociation time is several orders of magnitude slower than the radical's rotational period, for radicals formed with only 1 kcal/mol of vibrational energy above the barrier and comparable to the rotational period for radicals formed with a vibrational energy of 35 kcal/mol above the zero-point level.) C−O bond fission in rotationally excited CH_2CH_2OH radicals gives ethene and OH products with high tangential recoil velocities, with the distribution in Figure 8 peaking near 15 kcal/mol. We use an impulsive rotational model (also used in our previous work to determine the vibrational energy distribution of the nascent CH_2CH_2OH radicals) to predict the tangential recoil velocity that should be imparted to the OH and ethene fragments. The total recoil translational energy distribution for Br + unstable CH_2CH_2OH radicals peaks at E_T = 33 kcal/mol. In an impulsive model, the energy imparted into rotation is related to the recoil translational energy by the equation $E_{rot} = (\mu b^2/I)E_T$, where μ is the reduced mass of the CH_2CH_2OH + Br system, b is the impact parameter, and I is the moment of inertia about the axis of rotation of the CH_2CH_2OH radical. Photodissociation of the conformer of 2-bromoethanol that is trans about both the C−C bond and the C−O bond, results in CH_2CH_2OH radicals with E_{rot} = 15.5 kcal/mol when E_T = 33 kcal/mol. At the geometry of the transition state from CH_2CH_2OH to OH + ethene calculated by Senosiain et al.,[2] if all of the rotational energy is imparted to the tangential velocity of the fragments, C−O bond fission would then impart a tangential recoil energy of 17.1 kcal/mol. This is in rough agreement with the peak of the experimentally determined $P(E_T)$ shown in Figure 8, providing further validation that the impulsive model accurately characterizes the partitioning to rotational energy in the radical. In addition to signal from this secondary dissociation process, the m/e = 28 spectra also includes a contribution from the dissociative ionization of stable CH_2CH_2OH radicals, shown by the solid blue line, and a possible contribution from the dissociative ionization of m/e = 44 photofragments from HBr elimination from 2-bromoethanol, shown by the dashed purple line.

In Figure 10, the spectrum for OH products detected at m/e = 17 is shown with the forward convolution fit using the same primary and secondary $P(E_T)$'s that fit the momentum-matched ethene signal at m/e = 28.

C. Detection of Ethenol/Acetaldehyde Products at *m/e* = 44. CH_2CH_2OH radicals with sufficient vibrational energy can dissociate to mass 44 products via two possible pathways: a direct dissociation across a 33.1 kcal/mol barrier to ethenol + H or dissociation to acetaldehyde + H by first isomerizing across a 31.9 kcal/mol barrier to OCH_2CH_3. We expect that branching to the acetaldehyde + H channel will be minor because, after the isomerization to OCH_2CH_3, there is a lower energy pathway to CH_3 + H_2CO (discussed in section D). With the tunable VUV synchrotron ionization we can selectively detect the ethenol (IE = 9.3 eV) and acetaldehyde products (IE = 10.2 eV). At ionization energies below 10.2 eV, all of the detected m/e = 44 products are ethenol. The time-of-flight distribution shown in Figure 11 was taken at 9.2 eV and shows a forward convolution fit under the assumption that all unstable CH_2CH_2OH radicals + Br, as determined in our imaging experiments, have equal probability of dissociating to H + ethenol. As expected, on average, the internal energy distribution of the radicals that dissociate to ethenol + H is higher than that predicted for all C−Br bond fission events (and the corresponding velocity of the ethenol products slower, reflecting the dissociation of the slower, highly excited CH_2CH_2OH radicals). The fit is slightly too slow, but acceptable given the sensitivity to small variations in the ion flight constant and the short flight distance at the NSRRC. The slight mismatch of the fit with the data may also indicate that the

dx.doi.org/10.1021/jp203127k |J. Phys. Chem. A 2011, 115, 9097–9110

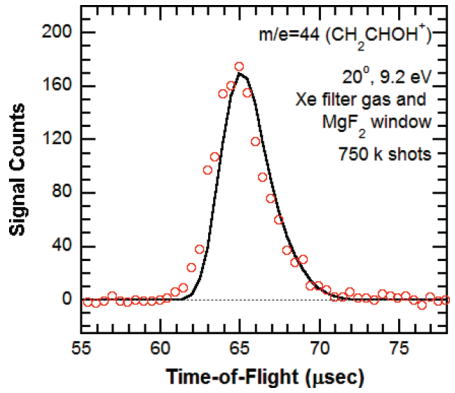

Figure 11. Time-of-flight spectrum at m/e = 44 (CH_2CHOH^+), detected with 9.2 eV photoionization. The open circles correspond to the data points, and the solid line is the fit predicted from the $P(E_T)$ for unstable CH_2CH_2OH + OH measured in our imaging experiments and shown as the green solid line in Figure 2.

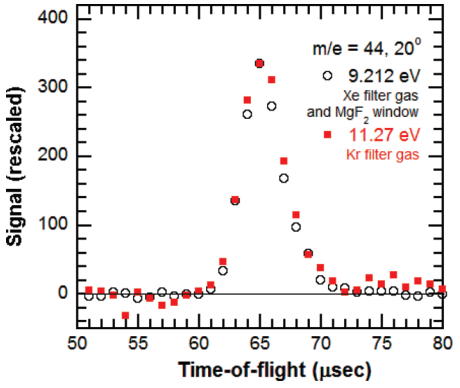

Figure 12. Time-of-flight spectrum at m/e = 44 with 9.2 eV (black circles) and 11.27 eV (red squares). At both ionization energies, the m/e = 44 signal from dissociation of CH_2CH_2OH radicals to ethenol + H can be detected. However, at a detection energy of 11.27 eV, acetaldehyde products may also contribute to the m/e = 44 signal. We would expect the ethenol and acetaldehyde products to have differing velocity distributions, which reflect the differing pathways to dissociation. The lack of change in the shape of the time-of-flight at indicates that majority of the detected m/e = 44 signal at 11.27 eV is ethenol products, not acetaldehyde.

percent of unstable radicals that dissociate to the H + ethenol channel is not uniform over the unstable radical + Br $P(E_T)$ distribution. However, one would expect that CH_2CH_2OH radicals formed with higher vibrational energy (lower translational energy) would have a higher branching to the H + ethenol product channel than those formed with lower vibrational energy (higher translational energies), effectively shifting the data slower than the fit; such a shift could not account for the error in the fit.

A time-of-flight spectrum at m/e = 44 (Figure 12) with 11.27 eV photoionization allows for the detection of both ethenol and acetaldehyde products. As shown in Figure 12, it is indistinguishable from the time-of-flight spectrum taken at 9.2 eV, supporting the conclusion that the m/e = 44 signal is primarily from the ethenol + H product channel. Based on the potential energy surface calculated by Senosiain et al.,[2] branching to the acetaldehyde + H channel is more significant from the subset of CH_2CH_2OH radicals formed with lower vibrational energies, i.e., higher recoil kinetic

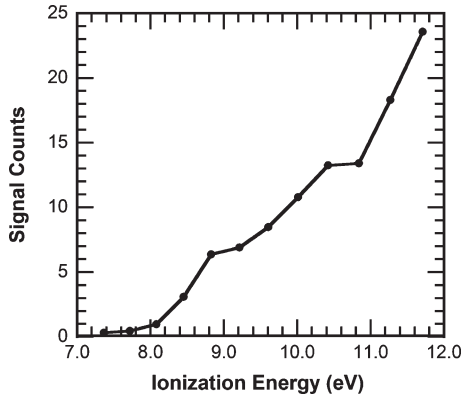

Figure 13. Low-resolution photoionization efficiency curve of m/e = 44 (CH_2CHOH and CH_3CHO) signal from the dissociation of CH_2CH_2OH radicals formed from the photodissociation of 2-bromoethanol at 193 nm. This spectrum is corrected for the NSRRC photon intensity as described in the Experimental Method section. The onset of signal at 8.4 eV corresponds to the ionization of vibrationally excited ethenol products with the broad bandwidth of the NSRRC synchrotron radiation. The lack of a sharp onset at 10.2 eV indicates that the H + acetaldehyde product asymptote is at most a minor channel. On the basis of the appearance energies in Table 1, the increase noted at 10.5 eV is likely from the dissociative ionization of mass 45 photofragments to m/e = 44.

energies. Thus, the detection of acetaldehyde signal in addition to the ethenol signal should shift the 11.27 eV, m/e = 44 time-of-flight to slightly faster times than the 9.2 eV spectra. The lack of change in the shape of the time-of-flight at 9.2 eV versus 11.27 eV indicates that the amount of acetaldehyde products is quite small.

Finally, we consider two additional sources of m/e = 44 signal: dissociative ionization of stable CH_2CH_2OH radicals (mass 45) and mass 44 products from the second primary dissociation channel (HBr loss from 2-bromoethanol). The appearance energy of m/e = 44 from stable CH_2CH_2OH radicals is 10.5 eV, so if stable radicals were dissociatively ionizing to m/e = 44, this should be observed in the 11.27 eV spectrum but not the 9.2 eV spectrum. The 11.27 eV spectrum has slightly more signal on the slow edge of the time-of-flight, which may be from the dissociative ionization of CH_2CH_2OH to m/e = 44. Additionally, it may also explain the increase in signal at energies above 10.8 eV in the PIE curve for m/e = 44 shown in Figure 13. As described in section A.3, the data taken at the NSRRC indicate that ~2% of the 2-bromoethanol parent molecules undergo HBr elimination upon photodissociation with 193 nm light. In our ongoing study of 2-bromoethanol-1,1,2,2-d_4, we detected both m/e = 83 (DBr^+) and m/e = 82 (HBr^+) products, suggesting the mass 44 coproducts to HBr in this current study are both ethenol and acetaldehyde. It is important to note that ethenol coproducts from HBr elimination could have significantly more internal energy than those formed from the secondary dissociation of CH_2CH_2OH radicals. This source of ethenol may contribute to the signal in the photoionization efficiency curve below 9.3 eV discussed in the next paragraph. The m/e = 44 fragments that are momentum-matched to m/e = 82 (HBr^+) are shown in dashed purple line in the Supporting Information. It is clear that most of the m/e = 44 signal is not from this channel, but from the ethenol product channel of the CH_2CH_2OH radicals.

We attempt to measure the relative signal intensity from the ethenol and acetaldehyde isomers by measuring the photoionization efficiency (PIE) curve of the total m/e = 44 signal, as

shown in Figure 13. The PIE curve has been adjusted for the photocurrent intensity as described below. At a given ionization energy the measured ionization cross section for a sample containing both ethenol and acetaldehyde is a linear combination of the photoionization cross sections for pure ethenol and pure acetaldehyde weighted by their mole fractions. If we used a high resolution ionization source and the mass 44 products were vibrationally cold, we would expect to see an onset of signal at 9.3 eV for ethenol products and a steep, sharp increase at 10.2 eV from the ionization of acetaldehyde products (similar to that observed in flames by Cool et al.[18]). Our m/e = 44 PIE curve shows an onset of signal at 8.4 eV that steadily increases until 11 eV, at which point there is a steep increase until 12 eV (see the Supporting Information for the PIE curve beyond 12 eV). Because the NSRRC bandwidth is considerably broader than that used in the high resolution experiments, we measured the PIE curve for pure acetaldehyde at the NSRRC, shown in the Supporting Information, from 8.4 to 12.7 eV. We convolute the high-resolution PIE curve measured by Cool et al. with the NSRRC bandwidth[24,32] for comparison. The agreement is excellent until 10.8 eV, at which point the synchrotron gives a larger relative photoion signal, likely from a higher photon flux at the higher energies. This allows us to determine the change in photon intensity as a function of energy. The PIE curve shown in Figure 13 was adjusted for this change in photon intensity. Despite the broad bandwidth, it is clear that a sharp increase in signal starting at 10.2 eV should be seen with the ionization of acetaldehyde products. Because we were unable to measure a PIE curve for pure ethenol, we convoluted the bandwidth of the NSRRC with the derived PIE curve of ethenol published by Cool et al.[18] The broad bandwidth negligibly affects this PIE curve, as shown in the Supporting Information. Thus, the onset of signal at 8.4 eV, and gradual increase until 10.8 eV, indicates the ionization of vibrationally hot ethenol products. The lack of a sharp increase near 10.2 eV indicates that acetaldehyde is at most a minor product channel. The red shift of the observed PIE curve does not make it feasible to quantitatively determine the branching to the ethenol + H and acetaldehyde + H product channels with the method used by Cool et al.[18] However, the measured PIE curve provides a clear indication that ethenol products are produced and that less than a third of the total m/e = 44 signal is from acetaldehyde products.

D. Detection of $H_2CO + CH_3$ at m/e = 15 and m/e = 30. The CH_2CH_2OH radicals that isomerize via the 31.9 kcal/mol barrier to OCH_2CH_3 may undergo C−C bond fission to form H_2CO + CH_3 products. The H_2CO signal was detected at m/e = 30 as shown in Figure 14 with the fit predicted from the $P(E_T)$ in Figure 15 for $CH_2CH_2OH \rightarrow H_2CO + CH_3$, assuming a $1/\sin(\theta)$ angular distribution for this secondary process as shown in Figure 9. (Again, the expected isomerization/dissociation time of the radical is on average longer than the rotational period of the radical.) The total signal near a time-of-flight of 70 μs in Figure 14 is too large to be accounted for by the backward scattered peak expected for the dissociation of a rotationally excited CH_2CH_2OH radical. We could not identify the source of this signal, shown as a short dashed orange line in Figure 14. We nevertheless fit the remaining signal in Figure 14 to the dissociation of CH_2CH_2OH to H_2CO + CH_3 products with a $1/\sin(\theta)$ angular distribution, but in our estimate of error bars in the calculated branching ratios, we explicitly allow for the possibility that the angular distribution could be isotropic, as shown in the Supporting Information. The m/e = 30 signal also

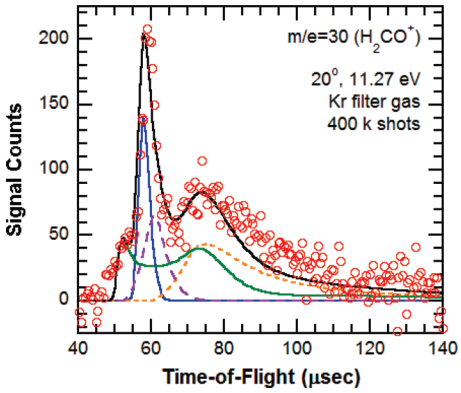

Figure 14. Time-of-flight spectrum at m/e = 30 (H_2CO^+) with 11.27 eV. The data are shown as open circles, and the solid black line represents the overall fit. The overall fit contains contributions from four sources. The fit given by the solid green line corresponds to H_2CO products formed from the isomerization of CH_2CH_2OH radicals to ethoxy and subsequent C−C bond fission to form H_2CO + CH_3 products. The $P(E_T)$ and angular distribution that gave this fit are shown in Figures 15 and 9, respectively. The fit shown by the solid blue line is from dissociative ionization of stable CH_2CH_2OH radicals, and the contribution given by the dashed purple line is from the dissociative ionization of m/e = 44 photofragments from HBr elimination from 2-bromoethanol. The fit shown as the short dashed orange line is unidentified signal from dissociative ionization that is also a minor contributor to the signal in the m/e = 15 spectrum.

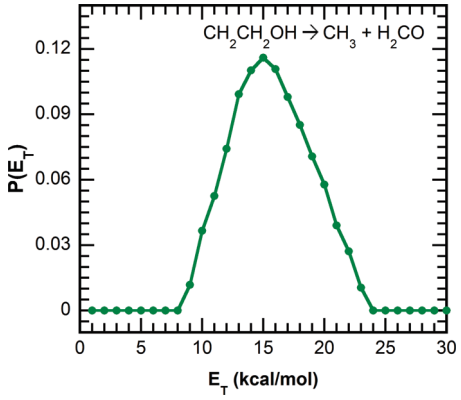

Figure 15. Recoil kinetic energy distribution for $CH_2CH_2OH \rightarrow CH_3$ + H_2CO derived from forward convolution fitting of the m/e = 30 (H_2CO^+) and m/e = 15 (CH_3^+) data shown as solid green lines in Figures 14 and 16, respectively. In the forward convolution fitting, this $P(E_T)$ has a $1/\sin(\theta)$ angular distribution as shown in Figure 9.

contains a contribution from the dissociative ionization of stable CH_2CH_2OH radicals, which is shown by the solid blue line, and a possible contribution from the dissociative ionization of m/e = 44 photofragments from HBr elimination of 2-bromoethanol, shown by the dashed purple line. We believe this signal is from multiphoton processes. The spectrum for CH_3 products detected at m/e = 15 is shown in Figure 16 with the predicted momentum-matched signal to the m/e = 30 data shown in Figure 14.

E. Detection of C_2H_3 Products at m/e = 27. Though H_2O + vinyl is a product channel expected from the direct abstraction channel of OH + ethene, it is not expected from the addition mechanism. We were surprised to detect m/e = 27 signal at

dx.doi.org/10.1021/jp203127k |J. Phys. Chem. A 2011, 115, 9097–9110

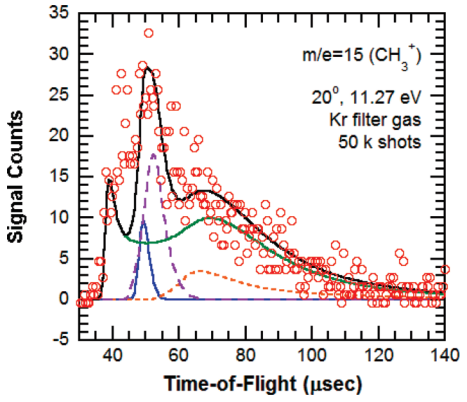

Figure 16. Time-of-flight spectrum at m/e = 15 (CH_3^+) with 11.27 eV. The data are shown as open circles, and the solid black line represents the overall fit. The overall fit contains contributions from four sources. The fit given by the solid green line corresponds to CH_3 formed from the dissociation of CH_2CH_2OH radicals to H_2CO + CH_3 and is momentum-matched to that shown as the solid green line in Figure 14. The fit shown by the solid blue line is from dissociative ionization of stable CH_2CH_2OH radicals, and the contribution given as the dashed purple line is from the dissociative ionization of m/e = 44 photofragments from HBr elimination from 2-bromoethanol. The fit shown by the short dashed orange line is unidentified signal from dissociative ionization that is also a contribution to the signal in the m/e = 30 spectrum.

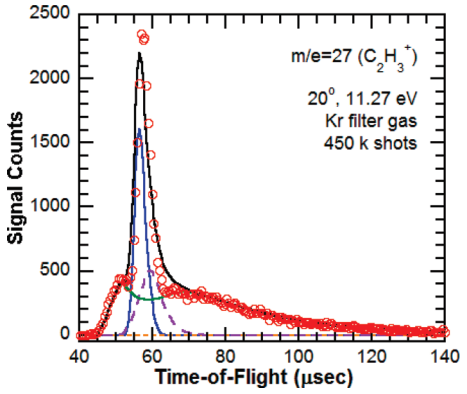

Figure 17. Time-of-flight spectrum at m/e = 27 (CH_2CH^+). The data are shown in open circles, and the overall fit is the black solid line. The solid green line shows the fit for signal resulting from the dissociation of CH_2CH_2OH to H_2O + vinyl with $P(E_T)$ shown in Figure 18 and $1/\sin(\theta)$ angular distribution in Figure 9. The solid blue line and dashed purple lines represent signals from dissociative ionization of stable CH_2CH_2OH radicals and mass 44 products from HBr elimination of 2-bromoethanol, respectively.

11.27 eV; we assign the signal fit by the green solid line in Figure 17 to vinyl from the H_2O + vinyl product channel. (The appearance energy for m/e = 27 ions from ethene is much higher, 12.4 eV.) The $P(E_T)$ for $CH_2CH_2OH \rightarrow H_2O$ + vinyl in Figure 18 was obtained by forward convolution fitting of the signal in Figure 17. The detection of the vinyl signal is unexpected because prior statistical treatments had not identified a low energy transition state connecting the CH_2CH_2OH radical adduct and H_2O + vinyl. The only route to H_2O + vinyl was the abstraction reaction of OH with ethene, but our experiments begin at the CH_2CH_2OH adduct. A single pass of the PIE curve

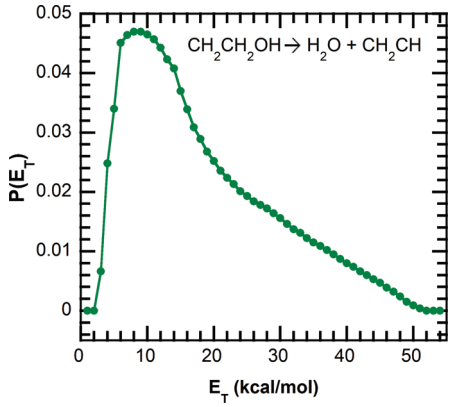

Figure 18. Recoil kinetic energy distribution for $CH_2CH_2OH \rightarrow H_2O$ + vinyl derived from forward convolution fitting the m/e = 27 (CH_2CH^+) signal in Figure 17.

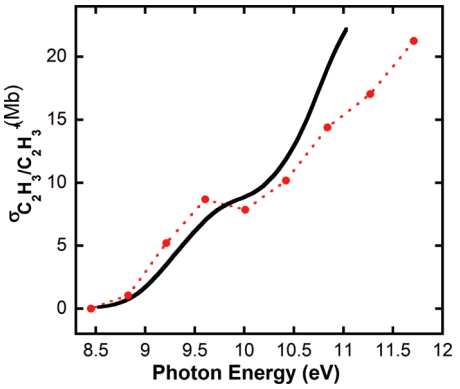

Figure 19. Photoionization efficiency curve at m/e = 27 (CH_2CH^+) from 8.45 to 11.71 eV shown as solid red circles and the dashed line. Shown for comparison as the solid black line is the broad-bandwidth averaged PIE curve measured by Taatjes et al.[33] The agreement confirms the assignment of the m/e = 27 signal shown by green solid line in Figure 17 to vinyl.

at m/e = 27 shown as solid red circles and the dashed line in Figure 19 agrees quite well with that measured by Taatjes and coworkers[33] (black solid line) for vinyl.

A year later, we revisited the NSRRC to detect H_2O, the momentum-matched cofragment to vinyl. As shown by the green solid line in Figure 20, the signal at m/e = 18 is qualitatively momentum-matched to the vinyl signal. This second set of data taken at the NSRRC proved even more difficult to analyze than the first. As shown in the Supporting Information, the m/e = 79 (Br^+) signal does not fit as a function of angle, which again suggests that the molecular beam velocity is not well characterized. As the m/e = 18 (H_2O^+) signal is not used in section F to determine the product branching, we settle for the fit in Figure 20, which confirms the detection of H_2O as the momentum-matched cofragment to vinyl.

F. Branching to OH + C_2H_4, H_2CO + CH_3, H_2O + C_2H_3, Ethenol + H, and Acetaldehyde + H Channels. These experiments, combined with our previous work, probe all of the final products for the nascent CH_2CH_2OH radicals formed from the 193 nm photodissociation of 2-bromoethanol. The channels resulting from the entire quantum yield of nascent radicals (from

dx.doi.org/10.1021/jp203127k |J. Phys. Chem. A 2011, 115, 9097–9110

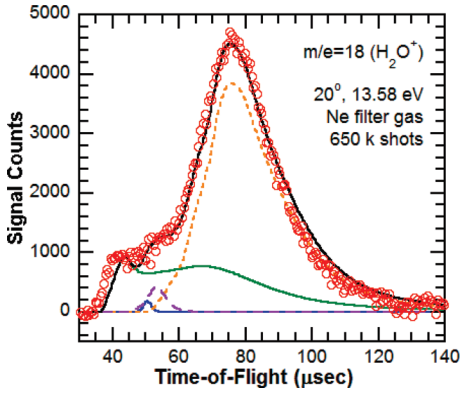

Figure 20. Time-of-flight spectrum at $m/e = 18$ (H_2O^+) with 13.58 eV detection taken at the NSRRC one year following the previous experiments. The data are shown as open red circles, and the total fit is the black solid line. The fit given as the solid green line is momentum-matched to the $m/e = 27$ signal shown as the solid green line in Figure 17 and obtained via forward convolution of the $P(E_T)$ in Figure 18 with the $1/\sin(\theta)$ angular distribution given in Figure 9. The fits given by the solid blue line and dashed purple lines represent signals from dissociative ionization of stable CH_2CH_2OH radicals and mass 44 products from HBr elimination of 2-bromoethanol, respectively. The signal shown as the dashed orange line is from clusters that were also detected at the parent mass of 2-bromoethanol of $m/e = 124$ (shown in the Supporting Information). The overall fit shows qualitatively that unexpectedly the H_2O + vinyl products do form, despite there being no direct pathway from the CH_2CH_2OH radical adduct. The mismatch of the fit at the fast edge is a testament to the difficulties in calibrating our molecular beam velocity and experimental parameters: ion flight constant and neutral beam path.

C−Br bond fission) is the sum of several channels:

$$1 = \Phi_{\text{stable}} + \Phi_{C_2H_4 + OH} + \Phi_{H_2CO + CH_3} + \Phi_{C_2H_3 + H_2O} + \Phi_{\text{ethenol+H}} + \Phi_{\text{acetaldehyde+H}}$$

where Φ_{products} is the quantum yield for each product channel. In our imaging experiments, we determined that 62% of all C−Br bond fission events resulted in Br + stable CH_2CH_2OH radicals, thus $\Phi_{\text{stable}} = 0.62$. On the basis of our results in section C, we attribute all the $m/e = 44$ signal to ethenol products and thus take $\Phi_{\text{acetaldehyde+H}} = 0$. We determine the branching between the $H_2CO + CH_3$, $OH + C_2H_4$, and $H_2O + C_2H_3$ product channels by measuring the relative signal intensities at $m/e = 30$, 28, and 27 detected with 11.27 eV ionization by alternating between the respective masses for a total of 400k laser shots to average out drifts in beam intensity, etc. We then integrate the components of each spectrum (shown in green solid line in Figures 7, 14, and 17) to account for the fraction of the total signal in the TOF at each m/e that results from each radical dissociation channel (rather than from other sources such as dissociative ionization of stable radicals). The integrated signal is adjusted for the expected signal sensitivity due to differing kinematic and Jacobian factors (including transit time through the ionizer) and the partial photoionization cross section, which is the product of the total photoionization cross section and the fraction of ionized species that appear at (in this case) the parent ion. The relative partial photoionization cross sections at 11.27 eV for $C_2H_4^+/C_2H_4$, $C_2H_3^+/C_2H_3$, and H_2CO^+/H_2CO are 8.14 Mb,[34] 22.32 Mb,[33] and 4.2 Mb,[32] respectively. Using a $1/\sin(\theta)$ secondary angular distribution for the product channels, the relative quantum yields are

$$\frac{\Phi_{H_2CO + CH_3}}{\Phi_{C_2H_4 + OH}} = \left(\frac{\text{integrated counts at } H_2CO^+}{\text{integrated counts at } C_2H_4^+}\right) \times \left(\frac{\text{expected } C_2H_4^+ \text{ signal}}{\text{expected } H_2CO^+ \text{ signal}}\right)\left(\frac{\sigma_{C_2H_4^+/C_2H_4}}{\sigma_{H_2CO^+/H_2CO}}\right) = \left(\frac{2586}{67435}\right)\left(\frac{33052}{29904}\right)\left(\frac{8.14}{4.2}\right) = 0.082$$

One possible source of error in the above branching ratio is the partial photoionization cross section of H_2CO to parent ion. Although 11.27 eV is below the appearance energy of HCO^+ from H_2CO, the Supporting Information shows our detected signal at HCO^+. Assuming the fragmentation pattern is the same in both experiments, the partial photoionization cross section ratio as used here is correct, so the fragmentation does not introduce error into the current analysis.

$$\frac{\Phi_{C_2H_3 + H_2O}}{\Phi_{C_2H_4 + OH}} = \left(\frac{\text{integrated counts at } C_2H_3^+}{\text{integrated counts at } C_2H_4^+}\right) \times \left(\frac{\text{expected } C_2H_4^+ \text{ signal}}{\text{expected } C_2H_3^+ \text{ signal}}\right)\left(\frac{\sigma_{C_2H_4^+/C_2H_4}}{\sigma_{C_2H_3^+/C_2H_3}}\right) = \left(\frac{32500}{67435}\right)\left(\frac{33052}{30702}\right)\left(\frac{8.14}{22.32}\right) = 0.19$$

Similarly, we determine the branching between C_2H_4 + OH and ethenol + H by measuring relative signal intensities for $m/e = 28$ and 44 at 10.5 eV by alternating between each m/e for a total of 400 k laser shots. The absolute partial photoionization cross sections at 10.5 eV for $C_2H_4^+/C_2H_4$ and CH_2CHOH^+/CH_2CHOH are 2.05 Mb[34] and 9.52 Mb,[18] respectively.

$$\frac{\Phi_{CH_2CHOH+H}}{\Phi_{C_2H_4+OH}} = \left(\frac{\text{integrated counts at } CH_2CHOH^+}{\text{integrated counts at } C_2H_4^+}\right) \times \left(\frac{\text{expected } C_2H_4^+ \text{ signal}}{\text{expected } CH_2CHOH^+ \text{signal}}\right) \times \left(\frac{\sigma_{C_2H_4^+/C_2H_4^+}}{\sigma_{CH_2CHOH^+/CH_2CHOH}}\right) = \left(\frac{887}{9904}\right)\left(\frac{1979}{1103}\right)\left(\frac{2.04}{9.515}\right) = 0.034$$

The integrated counts at $m/e = 44$ at 10.5 eV could include a modest contribution from signal due to HBr elimination from 2-bromoethanol.

The branching to the five product channels, combined with our previously measured stable radical distribution, determines the overall branching for the nascent CH_2CH_2OH radicals. As expected, the dominant product channel from these radicals is the OH + ethene channel with 76.5% of the reactive CH_2CH_2OH radicals undergoing C−OH bond fission. The rest of the dissociating CH_2CH_2OH radicals go on to product channels accessible to the reactive collision of OH + ethene; the measured branching fractions to those channels are given in Table 2. The largest source of uncertainty in the experimental branching ratios is from the error bars of the photoionization cross sections. Cool et al.[18] estimate that the error bar for the photoionization cross section for ethenol at 10.5 eV is ±26%.

Table 2. Relative Branching of the CH_2CH_2OH Radicals That Dissociate to One of the OH + Ethene Product Channels[a]

product channel	percent branching
$C_2H_3 + H_2O$	62.0
$H_2CO + CH_3$	26.8
ethenol + H	11.2

[a] Of the unstable radicals, branching to one of the three product channels accounts for 23.5% of the unstable CH_2CH_2OH radical adducts. The other 76.5% of unstable CH_2CH_2OH radicals dissociate to the OH + ethene reaction asymptote.

The error bars for the photoionization cross section for ethene at 11.27 eV are small, while the error bars for the vinyl cross section at 11.27 eV are roughly ±20%. While the error in formaldehyde's absolute cross section is roughly 20%, the photoionization cross section at 11.27 eV was determined from a ratio of signal in an experiment[31] where vinyl and formaldehyde were formed in a 1:1 ratio. Thus the ratio between the formaldehyde photoionization cross section and the vinyl photoionization cross section at 11.27 eV is more precise, ±12%.

DISCUSSION AND CONCLUSIONS

To our knowledge, this is the first complete study of the product branching from the CH_2CH_2OH adduct in the addition mechanism for the reaction of OH and ethene. Our relative integrated product signal at m/e = 44 (acetaldehyde and ethenol), m/e = 30 (H_2CO^+), m/e = 28 ($C_2H_4^+$), and m/e = 27 ($C_2H_3^+$) proved insensitive to the errors in the calibration parameters used for this analysis. We generated the CH_2CH_2OH radical adduct with 193 nm photodissociation of 2-bromoethanol, resulting in the well-characterized vibrational energy distribution shown in Figure 1.[1] From this vibrational energy distribution, 62% of the CH_2CH_2OH radicals remained energetically stable (they did not undergo subsequent dissociation before being photoionized in the imaging experiments). Of the ones that did dissociate, 76.5% dissociated to the reactant asymptote of OH + C_2H_4, 14.5% formed $C_2H_3 + H_2O$, 6.3% formed $H_2CO + CH_3$, 2.6% formed H + ethenol, and <1% formed H + acetaldehyde.

The detection of an H_2O + vinyl product channel was surprising, as prior experimental work and statistical treatments had assigned this to a direct abstraction channel, not a channel accessible via an addition mechanism. However, because the dissociation of the CH_2CH_2OH radical to OH + ethene is over a flat region of the potential energy surface, we infer that during a trajectory out to OH + ethene that the OH group can recross and abstract an H atom to access the H_2O + vinyl product channel. Indeed, one would treat the dissociation to OH + ethene with variational transition state theory to identify the best dividing surface to minimize the recrossing of trajectories that are proceeding out the product asymptote but return to the CH_2CH_2OH radical adduct. Therefore, for such channels one might consider the possibility that trajectories that recross en route to OH + ethene might access the H_2O + vinyl product channel before returning to the radical well. We confirm the vinyl product channel with the PIE curve of m/e = 27 and the detection of the momentum-matched cofragment H_2O. Concurrent work by Bowman and co-workers[4] found trajectories originating from the CH_2CH_2OH radical adduct that make their way to vinyl + H_2O products in what appears to begin as a frustrated dissociation to OH + ethene. At 44.1 kcal/mol, their trajectory calculations find that the roaming pathway constitutes a minor (a few percent) channel of the overall CH_2CH_2OH dissociation.[4] Our experimental branching to the H_2O + vinyl channel is 14.5% from the entire vibrational distribution of dissociating radicals, most of which have vibrational energies below the barrier for H-atom abstraction. The trajectory results, if extended below 44.1 kcal/mol, would thus likely evidence an even smaller branching to that channel than a few percent as they currently do not include tunneling corrections. As our branching to that channel is much larger, we conclude that accounting for quantum tunneling may be necessary to accurately predict the observed branching to the H_2O + vinyl channel. It will be interesting to compare this pathway's dependence on tunneling by doing experiments on a partially deuterated precursor. In this study, when an H atom is abstracted to form H_2O + vinyl the relative signal intensity between m/e = 79 (Br^+) and m/e = 18 (H_2O^+), shown as the solid green line in Figure 20, was 1:0.35. In our ongoing work using 2-bromoethanol-1,1,2,2-d_4 as a photolytic precursor,[28] we observe signal at HDO^+ from the analogous pathway where the OH group abstracts a D atom from CD_2CD_2 to form HDO + CD_2CD.

Table 3. Statistical Predictions for Product Branching from CH_2CH_2OH Radical Adducts with the Vibrational Energy Distribution Shown in Reference 1 and in Figure 1

	possible vinyl + H_2O channel	no vinyl + H_2O channel
$H_2CO + CH_3$	0.84%	0.84%
CH_3CHO + H	0.01%	0.01%
C_2H_4 + OH	95.27%	96.86%
$HOCHCH_2$ + H	1.70%	2.29%
$C_2H_3 + H_2O$	2.18%	0.00%

We attempt to compare our experimental measurement of the product branching to that predicted with transition state theory. As there is no transition state[2] that links the CH_2CH_2OH radical adduct to the H_2O + vinyl product channel, we first use the transition states calculated by Senosiain et al.[2] to predict the branching to the OH + ethene, H + ethenol, H + acetaldehyde, and $H_2CO + CH_3$ product channels as if the H_2O + vinyl product channel did not occur. Using the Multiwell Program Suite[35] and allowing tunneling within a 1-D Eckart approximation, we average the predicted product branching over the distribution of vibrational energy for the CH_2CH_2OH radicals in Figure 1. (Note that, although the authors in ref 2 replace low frequency vibrations with free internal rotors, their Supporting Information does not give adequate information to reproduce those predictions. We therefore retain the low frequency modes as harmonic oscillators with the frequencies given in Table 4 of ref 2.) The results are shown in the last column in Table 3. The agreement with the experimental results is unsatisfactory. As our data reveal a substantial branching to the H_2O + vinyl product channel, we also tried an alternate prediction for the product branching by treating the OH + $C_2H_4 \rightarrow H_2O$ + vinyl transition state calculated by Senosiain et al.[2] as if it were the effective transition state between our radical adduct and H_2O + vinyl products. The resulting prediction is shown in the middle column in Table 3. While the inclusion of this pathway to vinyl + H_2O does increase the branching to this channel, it does not begin to account for the 14.5% branching that we observed. If we assume that trajectories

heading out to the OH + ethene product asymptote bifurcate between proceeding to OH + ethene or undergoing an abstraction to form H_2O + vinyl, we can make a further comparison with the statistical predictions. The sum of these two channels (76.5% + 14.5% = 91%) is much closer to the yield of OH + ethene predicted by the statistical theories. This is at best a very ad hoc description of the dynamics and resulting product branching. To obtain an accurate theoretical prediction to compare with our experimental measurement, one must start the prediction from the CH_2CH_2OH radical with the range of vibrational energy shown in Figure 1. We look forward to the new trajectory results of Bowman and co-workers that seek to include tunneling corrections. A full quantum dynamics treatment is prohibited by the number of degrees of freedom and the high vibrational energy in the radical intermediate. It is interesting to consider the possibility that the frustrated dissociation to OH + ethene that results in this source of H_2O + vinyl products may be influenced by the small van der Waals complex along the OH + $C_2H_4 \rightarrow CH_2CH_2OH$ reaction coordinate. Although ref 2 shows the direct abstraction transition state connected to the OH + ethene asymptote, electronic structure calculations on a similar system, OH + propene, suggest that direct abstraction occurs via the van der Waals complex.[36]

■ ASSOCIATED CONTENT

Supporting Information. TOF spectra, number density of the molecular beam velocity distribution, PIE curves, $P(E_T)$ vs E_T fits, photoionization efficiency curve, recoil kinetic energy distribution, and lists of branching fractions and calculated appearance energies of ions resulting from the dissociative ionization of the neutral product. This material is available free of charge via the Internet at http://pubs.acs.org.

■ ACKNOWLEDGMENT

This work was supported by the Chemical Sciences, Geosciences, and Biosciences Division, Office of Basic Energy Sciences, Office of Science, U.S. Department of Energy, under Grant No. DE-FG02-92ER14305 (L.J.B.). We also acknowledge supplemental support in collaboration with Steve Pratt by the University of Chicago and the Department of Energy under section H.35 of U.S. Department of Energy Contract No. DE.AC02-06CHl1357 awarded to UChicago Argonne, LLC, operator of Argonne National Laboratory. A National Science Foundation Graduate Research Fellowship supported B.J.R. Synchrotron beam time and additional funding were provided by the National Synchrotron Radiation Research Center (NSRRC) and Academia Sinica in Taiwan (J.M.L.). We gratefully acknowledge the assistance in data acquisition at the NSRRC provided by Wen-Jian Huang, Wei-Kan Chen, I-Cheng Chen, and Andrew F. Chen in 2010 and by Caroline Womack, Andrew F. Chen, and Chen-Hsun Tsai in 2011. We also thank Maya Fishbach (University of Chicago Lab School) for her assistance recoding the program to characterize the molecular beam velocity to include the additional slow signal observed in our TOF. We thank C. Taatjes for sharing his prepublication data on his OH + ethene bulk kinetics experiments.

■ REFERENCES

(1) Ratliff, B. J.; Womack, C. C.; Tang, X. N.; Landau, W. M.; Butler, L. J.; Szpunar, D. S. *J. Phys. Chem. A* **2010**, *114*, 4934.

(2) Senosiain, J. P.; Klippenstein, S. J.; Miller, J. A. *J. Phys. Chem. A* **2006**, *110*, 6960 and references therein.

(3) Hintsa, E. J.; Zhao, X.; Lee, Y. T. *J. Chem. Phys.* **1990**, *92*, 2280.

(4) Kamarchik, E.; Koziol, L.; Reisler, H.; Bowman, J. M.; Krylov, A. I. *J. Phys. Chem. Lett.* **2010**, *1*, 3058.

(5) Park, Y.; Kang, K.; Jung, S.; Choi, J. *J. Phys. Chem. A* **2010**, *114*, 4891.

(6) Edwards, L. W.; Ryazanov, M.; Resiler, H.; Klippenstein, S. J. *J. Phys. Chem. A* **2010**, *114*, 5453.

(7) Shubert, V. A.; Rednic, M.; Pratt, S. T. *J. Phys. Chem. A* **2009**, *113*, 9057.

(8) Atkinson, R.; Perry, R. A.; Pitts, J. N. *J. Chem. Phys.* **1977**, *66*, 1197.

(9) Tully, F. P. *Chem. Phys. Lett.* **1983**, *96*, 148.

(10) Tully, F. P. *Chem. Phys. Lett.* **1988**, *143*, 510.

(11) Hippler, H.; Viskolcz, B. *Phys. Chem. Chem. Phys.* **2000**, *2*, 3591.

(12) Cleary, P. A.; Baeza Romero, M. T.; Blitz, M. A.; Heard, D. E.; Pilling, M. J.; Seakins, P. W.; Wang, L. *Phys. Chem. Chem. Phys.* **2006**, *8*, 5633.

(13) Taatjes, C. A.; Hansen, N.; McIlroy, A.; Miller, J. A.; Senosiain, J. P.; Klippenstein, S. J.; Qi, F.; Sheng, L.; Zhang, Y.; Cool, T. A.; Wang, J.; Westmoreland, P. R.; Law, M. E.; Kasper, T.; Kohse-Höinghaus, K. *Science* **2005**, *308*, 1887.

(14) Taatjes, C. A.; Hansen, N.; Miller, J. A.; Cool, T. A.; Wang, J.; Westmoreland, P. R.; Law, M. E.; Kasper, T.; Kohse-Höinghaus, K. *J. Phys. Chem. A* **2006**, *110*, 3254.

(15) Hippler, H.; Klinger, M.; Krasteva, N.; Nasterlack, S.; Olzmann, M.; Striebel, F. *Proceedings of the European Combustion Meeting*, 2005. Hippler, S. H.; Klinger, M.; Nasterlack, S.; Olzmann, M.; Striebel, F., *Proceedings of the European Combustion Meeting*, 2007.

(16) Bartels, M.; Hoyermann, K.; Sievert, R. *Proc. Combust. Inst.* **1982**, *19*, 61.

(17) Srinivasan, N. K.; Su, M.-C.; Michael, J. V. *Phys. Chem. Chem. Phys.* **2007**, *9*, 4155.

(18) Cool, T. A.; Nakajima, K.; Mostefaoui, T. A.; Qi, F.; McIlory, A.; Westmoreland, P. R.; Law, M. E.; Poison, L.; Peterka, D. S.; Ahmed, M. *J. Chem. Phys.* **2003**, *119*, 8356.

(19) Wang, C. C.; Lee, Y. T.; Lin, J. J.; Shu, J.; Lee, Y. Y.; Yang, X. *J. Chem. Phys.* **2002**, *117*, 153.

(20) Lee, S.-H.; Lee, Y.-Y.; Lee, Y. T.; Yang, X. *J. Chem. Phys.* **2003**, *119*, 827.

(21) Lin, J. J.; Chen, Y.; Lee, Y. Y.; Lee, Y. T.; Yang, X. *Chem. Phys. Lett.* **2002**, *361*, 374.

(22) Lee, Y. T.; McDonald, J. D.; LeBreton, P. R.; Herschbach, D. R. *Rev. Sci. Instrum.* **1969**, *40*, 1402.

(23) Yang, X.; Lin, J.; Lee, Y. T.; Blank, D. A.; Suits, A. G.; Wodtke, A. M. *Rev. Sci. Instrum.* **1997**, *68*, 3317.

(24) FitzPatrick, B. L.; Maienschein-Cline, M.; Butler, L. J.; Lee, S.-H.; Lin, J. J. *J. Phys. Chem. A* **2007**, *111*, 12417.

(25) Daly, N. R. *Rev. Sci. Instrum.* **1960**, *31*, 264.

(26) Curtiss, L. A.; Redfern, P. C.; Raghavachari, K.; Pople, J. A. *J. Chem. Phys.* **2001**, *114*, 108.

(27) Curtiss, L. A.; Redfern, P. C.; Raghavachari, K. *J. Chem. Phys.* **2007**, *126*, 084108.

(28) Frisch, M. J.; Trucks, G. W.; Schlegel, H. B.; et al. *Gaussian 09*, Revision A.02; Gaussian, Inc.: Wallingford, CT, 2009.

(29) Womack, C. C.; Ratliff, B. J.; Butler, L. J.; Lee, S.-H.; Lin, J. J. Manuscript in preparation.

(30) Gallagher, J. W.; Brion, C. E.; Samson, J. A. R.; Langhoff, P. W. *J. Phys. Chem. Ref. Data* **1988**, *17*, 103.

(31) The photoionization cross section for Br($^2P_{3/2}$) near 15.34 eV is 50.4 Mb according to: Lin, D.; Saha, H. P. *Phys. Rev. A* **1999**, *59*, 3614. Assuming a statistical ratio for the cross section of Br($^2P_{1/2}$) to Br($^2P_{3/2}$) in this region, the photoionization cross section of Br($^2P_{1/2}$) is then 25.2 Mb. We weight these values by the spin-orbit branching ratio of 0.8:0.2 for Br($^2P_{3/2}$):Br($^2P_{1/2}$) to obtain the value of 45.4 Mb for the photoionization cross section of all Br atoms.

(32) FitzPatrick, B. L.; Alligood, B. W.; Butler, L. J.; Lee, S.-H.; Lin, J. J. *J. Chem. Phys.* **2010**, *133*, 094306.
(33) Taatjes, C. A. Private communication, 2008.
(34) Cool, T. A.; Wang, J.; Nakajima, K.; Taatjes, C. A.; Mcllroy, A. *Int. J. Mass. Spectrom.* **2005**, *247*, 18.
(35) (a) *MultiWell-2011 Software*, 2011, designed and maintained by John R. Barker with contributors N. F. Ortiz, J. M. Preses, L. L. Lohr, A. Maranzana, P. J. Stimac, T. L. Nguyen, and T. J. Kumar, University of Michigan, Ann Arbor, MI, http://aoss.engin.umich.edu/multiwell. (b) Barker, J. R. *Int. J. Chem. Kinet.* **2001**, *33*, 232. (c) Barker, J. R. *Int. J. Chem. Kinet.* **2009**, *41*, 748.
(36) Szori, M.; Fittschen, C.; Csizmadia, I.; Viskolcz, B. *J. Chem. Theory Comput.* **2006**, *2*, 1575.